Anal. Chem. **2000,** *72,* 669−679

Electrochemical Impedance Spectroscopy and X-ray Photoelectron Spectroscopy Study of the Response Mechanism of the Chalcogenide Glass Membrane Iron(III) Ion-Selective Electrode in Saline Media

Roland De Marco* and Bobby Pejcic

School of Applied Chemistry, Curtin University of Technology, GPO Box U 1987, Perth, Western Australia, 6845, Australia

The response mechanism of the iron(III) chalcogenide glass membrane ion-selective electrode (ISE) in saline media has been studied using electrochemical impedance spectroscopy (EIS) and X-ray photoelectron spectroscopy (XPS). EIS equivalent circuits and XPS surface compositions for the Fe^{III} ISE are consistent with the presence of two surface films probably comprising a outer surface layer (OSL) and an Fe-deficient modified surface layer (MSL), along with a low-frequency charge-transfer impedance that is attributable to the reduction of Fe^{3+}. In accordance with literature data for the conductivity of low-bearing iron(III) chalcogenide glasses, a high-impedance MSL is internally consistent with XPS data for an Fe-deficient MSL. It is evident that the impedance of the MSL diminishes on exposure to solutions containing Fe^{3+}, and this finding is consistent with the ion exchange of Fe^{3+} within the MSL. Likewise, the charge-transfer impedance also decreases at elevated levels of Fe^{3+}, demonstrating that Fe^{3+} is a participant in the reversible charge-transfer reaction occurring at the electrolyte/electrode interface. The kinetics of charge transfer are facilitated by Fe chelating agents (e.g., citrate, salicylate, EDTA, etc.) due presumably to the complexation of the products of the charge transfer process (possibly Fe^{2+}). It is shown unequivocally that the response of the Fe^{III} ISE in saline buffers is independent of pH, demonstrating that the ISE is responding directly to Fe^{3+}, not H^+. A mechanism involving a combination of charge transfer and ion exchange of Fe^{III}, at the electrode diffusion layer, has been proposed to explain the 30 mV/decade slope of the Fe^{III} ISE.

Vlasov, Bychkov and Legin[1] have developed a range of chalcogenide glass sensor materials including the Fe^{III} ion-selective electrode (ISE) that are highly durable, sensitive, and suitable for industrial and environmental monitoring. The chalcogenide glass membranes are resistant to attack by acidic and corrosive media and possess chemically stable surface characteristics. In addition, interferences from other ions are minimal, and the detection limit for most of these electrodes in unbuffered standards is $\sim 10^{-6}$ M[1].

A hindrance to the application of the iron(III) chalcogenide glass ISE for seawater analyses has been the contradictory reports in the literature regarding a physicochemical rationale for its response mechanism. Most workers agree that the mechanism is probably electronic rather than ionic.[2−4] Baker and Trachtenberg[2] and Vlasov and Bychkov[3,4] agreed that the mechanism involves electron exchange between deep-centered $Fe^{2+}(d^6)$ donors in the surface layers of the vitreous glass along with acceptor ions in solution (Fe^{3+}_L) and is represented by the following reaction:

$$Fe^{3+}_L + Fe^{2+}\,(d^6) \rightarrow Fe^{2+}_L + Fe^{3+}\,(d^5) \qquad \text{(I)}$$

The Mossbauer spectroscopy results for a membrane exposed to solution[3,4] revealed that the ratio of tetrahedrally coordinated Fe^{3+} to Fe^{2+} was higher than that for an untreated membrane, supporting the electron-transfer mechanism. In fact, the ISE potential varied as a function of $\log([Fe^{2+}]/[Fe^{3+}])$ but not $\log[Fe^{2+}]$, verifying a sensitivity of the Fe^{III} ISE to the Fe^{3+}/Fe^{2+} redox couple. By contrast, the potential is a function of $\log[Fe^{3+}]$ at fixed values of $\log([Fe^{2+}]/[Fe^{3+}])$, indicating that the response mechanism cannot be ascribed purely to an electron-transfer process. In any event, these apparently contradictory results verify that the iron(III) chalcogenide ISE exhibits some Fe^{III}/Fe^{II} redox sensitivity,[3,4] along with some direct sensitivity to Fe^{III} that the authors suggest is attributable to Fe^{III} ion exchange at the electrolyte/electrode interface.

Despite the consensus on the electron-transfer mechanism for Fe^{III} response of the iron chalcogenide glass electrode, there are several inconsistencies related to the slopes of Fe^{III} ISE response curves. For example, Koenig and Grabner,[5] Vlasov and Bychkov,[6] and De Marco and Mackey[7] have reported slopes of 30−50 mV/

(1) Vlasov, Y. G.; Bychkov, E. A.; Legin, A. V. *Talanta* **1994**, *41*, 1059−63.

(2) Baker, C. T.; Trachtenberg, I. *J. Electrochem. Soc.* **1971**, *118*, 571−6
(3) Vlasov, Y. G.; Bychkov, E. A. *Ion Sel. Electrode Rev.* **1987**, *9*, 5−93.
(4) Vlasov, Y. G.; Bychkov, E. A. *Hung. Sci. Instrum.* **1982**, *53*, 35−42.
(5) Koenig, C. E.; Grabner, E. W. *Electroanalysis* **1995**, *7*, 1090−4.
(6) Vlasov, Y. G.; Bychkov, E. A. *J. Electroanal. Chem.* **1994**, *378*, 278−84.
(7) De Marco, R.; Mackey, D. J. *Mar. Chem.*, in press.

10.1021/ac990603x CCC: $19.00
Published on Web 01/15/2000

decade change in aFe^{3+} in unbuffered Fe^{III} standards, although Nernstian predictions for the aforementioned one-electron-transfer process imply a slope of 59.16 mV/decade, while other authors[2,3] have reported the univalent slope of 60 mV/decade.

In an important study by Koenig and Grabner,[5] cyclic voltammetry (CV) and X-ray photoelectron spectroscopy (XPS) were used to study the response mechanism of the chalcogenide glass Fe^{III} ISE. This work demonstrated that the Fe^{III} ISE undergoes two distinct CV reduction peaks that are attributable to Fe^{3+} and Fe^{2+} states within the membrane, and the Fe^{III} ISE possesses an Fe depleted modified surface layer (MSL) that is ~8 nm in thickness. Regrettably, these authors proposed a mechanism that predicted incorrectly a Nernstian response of 60 mV/decade change in aFe^{3+}, not the 30−50 mV/decade slopes reported by themselves[5] and other authors[4,7] for membranes comprising $Fe_2Se_{60}Ge_{28}Sb_{12}$.

Recently, the $Fe_2Se_{60}Ge_{28}Sb_{12}$ chalcogenide glass membrane Fe^{III} ISE has been used to obtain a Nernstian response of 30 mV/decade over a range of 10^{-23}−10^{-1} M in saline iron(III) citrate standards[7] and unbuffered Fe^{III} standards.[5] De Marco and Mackey[7] have also used the chalcogenide glass membrane Fe^{III} ISE for the analysis of Fe^{3+} in organic-free, UV-oxidized seawater, yielding an ISE response that was internally consistent with the results of metal speciation calculations undertaken using the equilibria for inorganic complexation of Fe^{III} in seawater. Unfortunately, the apparent divalent response of 30 mV/decade is inconsistent with the slope expected for a trivalent ion such as Fe^{3+} (i.e., 20 mV/decade), or the one predicted using the one-electron-transfer mechanism proposed by other authors.[2,3]

In order for the Fe^{III} ISE to gain widespread acceptance by the marine science community for the analysis of Fe^{3+} in seawater, it is necessary to place the Fe^{III} ISE on a sound theoretical basis by developing a physicochemical rationale for electrode response in a complex medium like seawater. Previous work by De Marco and co-workers[8−10] involving electrochemical impedance spectroscopy (EIS) and XPS studies of the jalpaite copper(II) ISE in saline media has elucidated important mechanistic information pertaining to the ion-exchange and charge-transfer processes occurring at the electrolyte/electrode interface of this analytically important system. A similar study of the Fe^{III} ISE was deemed appropriate as the Fe^{III} ISE's response mechanism has not been investigated in detail using EIS and XPS, and it is believed that this system also undergoes a combined redox/ion-exchange response mechanism.

EXPERIMENTAL SECTION

Reagents and Solutions. Analytical grade reagents were used in all cases, and all solutions were prepared in ultrahigh-purity Milli-Q water.

Iron(III) buffer solutions were prepared through pH adjustment of solutions comprising 10^{-4} M $FeCl_3$, 10^{-2} M ligand (EDTA, citrate, and salicylate), and 0.6 M NaCl. The buffer pH was set using concentrated HCl or NaOH, and the pH was recorded using a combination glass electrode that had been calibrated in standard pH buffers. The MINTEQA2 software package, available at the Old Dominion University website http://www.cee.odu.edu/cee/model/model.html, and associated stability and ionization constants were used to determine the speciation of Fe^{III} in solution, in particular the relationship between pFe and pH.

Electrodes. Selenium, germanium, antimony, and iron powders were mixed in the following proportions, $Fe_2(Se_{60}Ge_{28}Sb_{12})_{98}$,[5] and heated for 24 h at 1050 °C in an evacuated quartz ampule. The resultant glass was annealed for 2 h at 240 °C to remove any excess stress within the glass. A section of chalcogenide glass was fashioned into a disk approximately 5 mm thick and 13 mm in diameter, and its outer surfaces were polished to a gloss finish. A rotating disk electrode (RDE) was prepared by attaching a threaded aluminum stub to the rear surface of the chalcogenide glass membrane using silver epoxy, and the entire assembly was subsequently encapsulated in a clear epoxy resin.

EIS Studies. EIS studies on RDE Fe^{III} ISEs (polished on Struers 1 mm diamond spray, and Struers red lubricant) were undertaken using an EG&G Princeton Applied Research model 6310 potentiostat equipped with a lock-in amplifier. The EIS spectra were recorded using an overpotential window of ±10 mV, and a frequency range of 100 kHz to 10 mHz. A conventional three-electrode cell was used in the EIS studies [viz., a RDE Fe^{III} ISE as the working electrode, a platinum counter electrode, and a saturated calomel electrode (SCE) as the reference]. The RDE was inserted into a single-element PINE electrode rotator (model AFCPRB). All EIS spectra were fitted to equivalent circuits using the equivalent circuit program of Boukamp,[11] and Kramers−Kronig transformations of impedance data were performed using the LEVM 7.1 software.[12]

XPS Studies. XPS was carried out on a model VG Escalab 220 IXL at the University of New South Wales using Al Kα X-rays. The Fe^{III} ISE surfaces were prepared for XPS by polishing on 1 200 grit emery paper, followed by Struers 1 μm diamond particles in conjunction with Struers red lubricant and a felt pad. Iron(III) ISE membranes were rinsed in a jet of ultrahigh-purity Milli-Q water prior to and after exposure to solution.

RESULTS AND DISCUSSION

EIS Studies. EIS was used to study the electrode kinetics of the Fe^{III} ISE in unbuffered and buffered media to elucidate the response mechanism of the electrode. This study explored the role of redox and ion-exchange reactions on the response of the Fe^{III} ISE.

Iron Response in Unbuffered Standards. EIS complex-plane impedance plots (not shown for all data sets as they are similar, except for sample spectra for the citrate buffer presented in Figure 3) for a RDE Fe^{III} ISE in $FeCl_3$ standards at pH 1 in 0.1 M KCl revealed high-frequency outer surface layer (OSL) and MSL impedances (see Table 1). Another semicircle at lower frequencies is attributable to a charge-transfer impedance (i.e., R_{CT}), noting that the rate of charge transfer is inversely proportional to the charge-transfer impedance. Importantly, the complex-plane impedance plot for a solution without added Fe^{III} also revealed a large charge-transfer impedance that is attributable to Fe^{III} ISE response to the 2×10^{-7} M level of iron impurity in the 0.1 M KCl

(8) De Marco, R. *Mar. Chem.* **1996**, *55*, 389−98.
(9) De Marco, R.; Cattrall, R. W.; Liesegang, J.; Nyberg, G. L.; Hamilton, I. C. *Anal. Chem.* **1992**, *64*, 594−8.
(10) De Marco, R.; Eriksen, R.; Zirino, A. *Anal. Chem.* **1998**, *70*, 4683−9.
(11) Boukamp, B. A. In *Equivalent Circuit, Users Manual*, 2nd ed.; University of Twente: Twente, The Netherlands, 1993.
(12) Macdonald, J. R. *CNLS (Complex Nonlinear Least Squares Immittance Fitting Program), LEVM Manual*, Ver. 7.1; Solartron Group Ltd., 1999.

Table 1. Boukamp Equivalent Circuit Parameters and Open Cell Potentials for a RDE Chalcogenide Fe^{III} ISE in Fe^{3+} Standards at 3000 rpm[a]

$[Fe^{3+}]$	R_{SOLN} (Ω)	Q_1 (Ω^{-1} s^n)	n_1	R_{OSL} (kΩ)	Q_2 (Ω^{-1} s^n)	n_2	R_{MSL} (kΩ)	Q_3 (Ω^{-1} s^n)	n_3	R_{CT} (kΩ)
blank at 2×10^{-7} M; $E = -50.2$ mV	neg[b]	9.8×10^{-7}	0.605	1.16	9.4×10^{-7}	0.812	20.4	9.7×10^{-6}	0.518	231
4×10^{-5} M; $E = 22.4$ mV	neg	1.0×10^{-6}	0.605	1.14	1.3×10^{-6}	0.802	22.4	1.2×10^{-5}	0.532	102
2×10^{-3} M; $E = 117.4$ mV	neg	1.0×10^{-6}	0.607	1.05	1.2×10^{-6}	0.783	16.7	2.3×10^{-5}	0.578	35.4
1×10^{-1} M; $E = 222.6$ mV	10.3	8.6×10^{-7}	0.622	1.02	1.1×10^{-6}	0.760	7.38	6.1×10^{-5}	0.495	13.4

[a] Note that $\Delta E/\Delta pFe = -31.9$, -55.9, and -61.9 mV/decade between 2×10^{-7} and 4×10^{-5}, 4×10^{-5} and 2×10^{-3}, and 2×10^{-3} and 1×10^{-1} M, respectively. This variation in slope is typical for the response of the iron(III) chalcogenide glass ISE in unbuffered Fe standards, as has been observed by various other authors.[2−5] [b] neg, negligible.

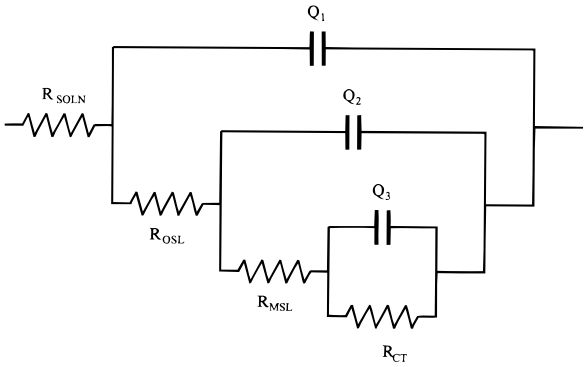

Figure 1. Equivalent circuit for the RDE Fe^{III} ISE that has been fitted using the Boukamp software program.

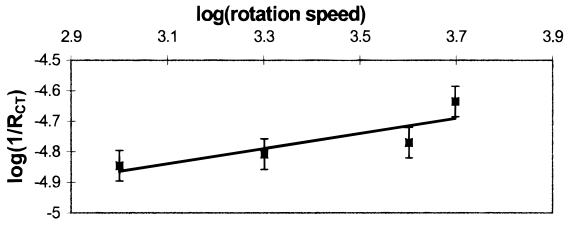

Figure 2. Levich equation plot of $\log(1/R_{CT})$ vs log(rotation speed) for the RDE Fe^{III} ISE in 10^{-3} M KCl containing 0.1 M KCl.

electrolyte (as determined by inductively coupled plasma mass spectrometry). It is worth noting that, in the context of this Fe-unspiked KCl medium, a previous cathodic stripping voltammetric study of corrosion of the iron(III) chalcogenide glass ISE[7] revealed that this ISE releases an insignificant amount of Fe (i.e., 8 nM total Fe is released into 10 mL of seawater over 5 min). The variation in charge-transfer impedance as a function of $[Fe^{3+}]$ (see Table 1) demonstrates that the kinetics of the charge-transfer process are dependent on Fe^{3+}, with the charge-transfer impedance of the Fe^{III} ISE diminishing at elevated levels of Fe^{3+} which favor the kinetics of the forward process of the reversible charge-transfer reaction.

The EIS spectra for the RDE Fe^{III} ISE in unbuffered Fe^{III} standards along with all other media utilized in this study were satisfactorily fitted to the equivalent circuit shown in Figure 1, yielding the equivalent circuit elements presented in Table 1. It is important to note that, in all media investigated in this study, the equivalent circuit for the electrolyte/membrane interface is characterized by four impedances (i.e., solution, OSL, MSL, and CT impedances), and Bode phase plots (also not shown) revealed the presence of at least three time constant circuit elements that we have employed as a criterion for fitting the latter of the aforementioned impedances using Boukamp equivalent circuit modeling. The three RC-type elements (OSL, MSL, CT) have been assigned in order of high-to-low frequency, as this is consistent with the expected kinetics of impedance response for rapid semi-infinite linear diffusion of Fe^{III} through a thin OSL, and to a lesser extent through a thicker MSL (i.e., ~20 nm as identified using XPS[5]), as opposed to the usual sluggish kinetics of charge transfer that normally prevail with ISEs.[13] Further credence for the proposed equivalent circuit is the XPS evidence (see Figure 5), which revealed a thick Fe-deficient MSL that is expected to have a relatively high impedance, on the basis of literature data for the variation in impedance for iron chalcogenide glasses as a function of Fe content.[5] The constant phase elements (CPE) Q_1, Q_2, and Q_3 are described by parameters n_1, n_2, and n_3 with resistances, Warburg terms, capacitances, and inductances being defined by $n = 0$, 0.5, 1, and -1, respectively.[11] It is worth noting that the n values of approximately 0.5 for the OSL and charge-transfer impedances are characteristic of Warburg diffusional terms;, i.e., the migration of Fe^{3+} within the OSL along with its effect on the corresponding charge-transfer reaction are under diffusion control. This observation implies strongly that the OSL impedance is attributable to semi-infinite linear diffusion of Fe^{III} through vacancies in the proposed MSL (as shown in the proposed ISE model in Figure 6).

The solution impedances in many instances (see Tables 1−8) are physically meaningless (i.e., very low or negative) due to limitations in measurements of EIS spectra coupled with deficiencies in the Boukamp equivalent circuit fitting procedure. It is important to note that high-frequency solution impedances are prone to noise pickup through stray capacitances,[14] and the Boukamp equivalent circuit algorithm is unable to reliably deconvolute a low value of solution impedance at high frequency (i.e., ~10 Ω) that is overlapped severely by large low-frequency OSL, MSL, and CT impedances in the vicinity of 1−100 kΩ. Despite these shortcomings, it is important to note that high

(13) Buck, R. P. In *Ion-Selective Electrodes in Analytical Chemistry*; Freiser, H., Ed.; Plenum Press: New York, 1978; pp 1−141.

(14) Macdonald, J. R.; Johnson, W. B. In *Impedance Spectroscopy Emphasizing Solid Materials and Systems*; Macdonald, J. R., Ed.; John Wiley and Sons: New York, 1987; pp 1−26.

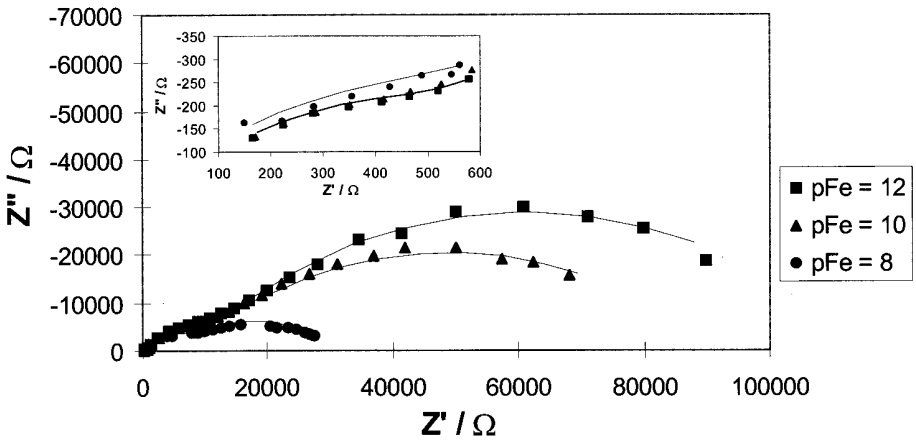

Figure 3. EIS complex-plane impedance plots for the Fe^{III} ISE in saline Fe^{III}-citrate buffered media at 3000 rpm. The high-frequency EIS response has been scale-expanded, as presented in the inset in the far left-hand corner of Figure 3.

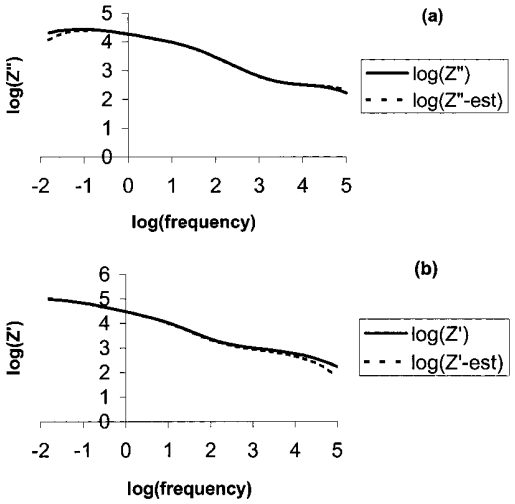

Figure 4. Kramers−Kronig transforms for an Fe^{III} ISE in a saline citrate buffer at pFe = 10: (a) log of imaginary impedance component [i.e., log(*Z*″)] vs log(frequency) for transformation of the real to the imaginary component; (b) log of real impedance component [i.e., log(*Z*′)] vs log(frequency) for transformation of the imaginary to the real component. Note that impedances estimated using Kramers−Kronig transformations are presented as broken lines.

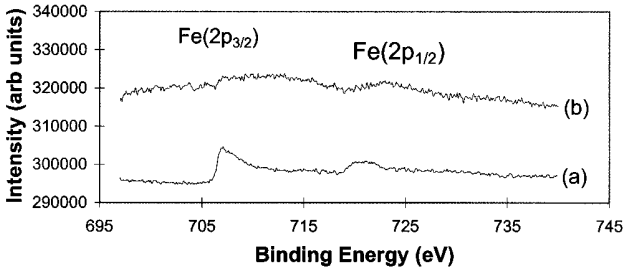

Figure 5. XPS spectra of the Fe(2p) levels for Fe^{III} ISE membranes: (a) a polished membrane after 200 s of argon ion etching; (b) a membrane exposed to an Fe^{III}-EDTA buffer at pFe = 20 for 3 days.

relative errors in estimated values of R_{soln} (i.e., <10 Ω) are insignificant in the context of the reliability of EIS data at moderate to low frequencies, which are the key EIS response regions for chemical processes occurring at the electrolyte/electrode interface.

Significantly, the OSL and MSL impedances also decrease at elevated levels of Fe^{3+}, and this diminution in impedance is symbolic of an ion-exchange process. Presumably, at elevated levels of Fe^{3+}, the OSL and MSL become more conductive as they are loaded with Fe^{III} ions. These findings strongly suggest that the response mechanism of the Fe^{III} ISE is attributable to a combination of electron-transfer and ion-exchange processes at the electrolyte/electrode interface.

The EIS spectra for a RDE Fe^{III} ISE in Fe^{2+} standards were also fitted to the equivalent circuit shown in Figure 1, yielding the equivalent circuit elements that are presented in Table 2. There are two notable features in the EIS data, i.e., a higher charge-transfer impedance and a more discernible MSL impedance compared to that with Fe^{3+} standards (compare Tables 1 and 2). In fact, the impedance of the MSL in Fe^{2+} standards is considerably higher than that for a corresponding level of Fe^{3+}. Furthermore, the charge-transfer impedance was at least double that for a corresponding level of Fe^{3+}. Despite the EIS evidence for Fe^{2+} undergoing ion exchange and charge transfer at the electrolyte/electrode interface, the much lower rates of charge transfer and ion exchange are symbolic of a kinetically less favored process. Potentiometric response measurements corroborate this finding as the Fe^{III} ISE does not display a significant response to Fe^{II} (compare potentials presented in Tables 1 and 2). It is clear that the MSL is selective toward Fe^{3+} as the MSL impedance is considerably larger in the presence of Fe^{2+}, and the electrode response mechanism follows the path of least resistance, noting that the electrode process is kinetically controlled under these conditions. The constancy in potential of the Fe^{III} ISE in the presence of variable levels of Fe^{2+} implies that there is no charge separation across the membrane/electrolyte interface, and this is probably attributed to the significant contribution by membrane dissolution in generating a constant level of Fe^{2+}. In fact, Mossbauer spectroscopy studies by Vlasov and Bychkov[4] have demonstrated that iron in the membrane is in the +2 oxidation state, and solubilization of this material is likely to yield a high and constant background level of Fe^{2+}.

The EIS data for a RDE Fe^{III} ISE in 10^{-3} M $FeCl_3$ also containing 0.1 M KCl at a range of rotation speeds were fitted to the equivalent circuit presented in Figure 1, yielding the Boukamp

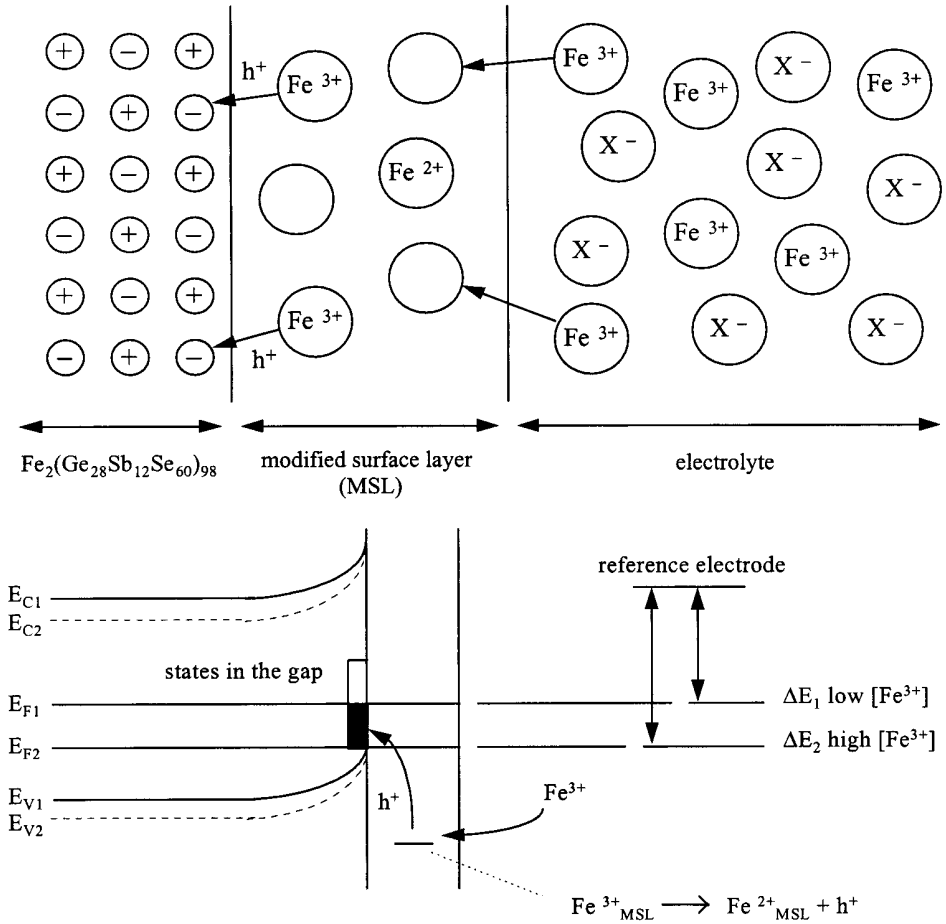

Figure 6. Schematic diagram of the electrolyte/electrode interface of the Fe^{III} ISE (Koenig and Grabner;[5] reproduced with the permission of the Editor-in-Chief of the VCH publication *Electroanalysis*). Note the following symbolism: E_C, energy of the conduction band; E_F, energy of the Fermi level; E_V, energy of the valence band. Scenario 1 is for low [Fe^{3+}], while situation 2 is for high [Fe^{3+}].

Table 2. Boukamp Equivalent Circuit Parameters and Open Cell Potentials for an RDE Chalcogenide Fe^{III} ISE in Fe^{2+} Standards at 3000 rpm

[Fe^{2+}]	R_{SOLN} (Ω)	Q_1 ($\Omega^{-1}s^n$)	n_1	R_{OSL} (kΩ)	Q_2 ($\Omega^{-1}s^n$)	n_2	R_{MSL} (kΩ)	Q_3 ($\Omega^{-1}s^n$)	n_3	R_{CT} (kΩ)
4×10^{-5} M; $E = -4.1$ mV	neg[a]	2.2×10^{-6}	0.544	1.33	1.5×10^{-6}	0.758	29.0	1.3×10^{-5}	0.641	198
2×10^{-3} M; $E = -3.1$ mV	neg	7.4×10^{-7}	0.637	1.04	2.3×10^{-6}	0.696	22.6	1.7×10^{-5}	0.580	103
1×10^{-1} M; $E = 1.6$ mV	neg	6.2×10^{-7}	0.651	0.951	1.4×10^{-6}	0.739	17.3	2.8×10^{-5}	0.502	46.1

[a] neg, negligible.

equivalent circuit elements that are presented in Table 3. As is expected for a diffusion-controlled process, the charge-transfer reaction of the Fe^{III} ISE is facilitated at elevated rotation speeds. A plot of $\log(1/R_{CT})$ versus log(rotation speed) is presented in Figure 2, and it reveals a slope of 0.3, which is close to the value of 0.5 predicted by the Levich equation for a RDE.[15] Although the Boukamp algorithm yields an estimate for most equivalent circuit parameters to a certainty of ±1−5%, excluding the Q terms, which can be in error by up to 30%, our experience has shown that electrode instability (drift of 1−10 mV during EIS measurements) degrades the reproducibility of Fe^{III} ISE EIS spectra to around ±10−20%. In any event, the small deviation in slope is probably attributed to geometrical irregularities and nonuniformities in the surface of the Fe^{III} ISE RDE.

Iron(III) Response in Buffered Media. EIS was carried out in buffered media to examine the influence of organic ligands on the response of the RDE Fe^{III} ISE. Figure 3 presents EIS complex-plane impedance plots for a RDE Fe^{III} ISE in Fe^{III}−citrate buffers, and the corresponding equivalent circuit elements are shown in Table 4. It can be seen that the rate of charge transfer, which is inversely proportional to R_{CT}, increases at elevated levels of free Fe^{III} in the citrate buffers. Significantly, the EIS data demonstrate

(15) Levich, V. *Physicochemical Hydrodynamics*; Prentice Hall: Englewood Cliffs, NJ, 1962.

Table 3. Boukamp Equivalent Circuit Parameters for a RDE Chalcogenide Fe^{III} ISE in 10^{-3} M $FeCl_3$ also Containing 0.1 M KCl as a Function of Rotation Speed

rotation speed (rpm)	R_{SOLN} (Ω)	Q_1 ($\Omega^{-1}s^n$)	n_1	R_{OSL} (kΩ)	Q_2 ($\Omega^{-1}s^n$)	n_2	R_{MSL} (kΩ)	Q_3 ($\Omega^{-1}s^n$)	n_3	R_{CT} (kΩ)
0	74.9	2.3×10^{-7}	0.735	0.273	1.7×10^{-6}	0.854	11.9	1.2×10^{-5}	0.446	114
1000	neg[a]	6.2×10^{-8}	0.789	0.307	2.1×10^{-6}	0.830	16.5	1.6×10^{-5}	0.526	70.1
2000	neg	1.0×10^{-7}	0.755	0.299	2.0×10^{-6}	0.843	13.1	1.7×10^{-5}	0.482	64.3
4000	neg	1.3×10^{-7}	0.736	0.319	2.0×10^{-6}	0.841	13.3	2.0×10^{-5}	0.464	58.9
5000	neg	1.2×10^{-7}	0.748	0.320	2.3×10^{-6}	0.828	14.4	3.0×10^{-5}	0.496	43.1

[a] neg, negligible.

Table 4. Boukamp Equivalent Circuit Parameters and Open Cell Potentials for a RDE Chalcogenide Fe^{III} ISE in Fe^{III}−Citrate Buffers and Seawater at 3000 rpm[a]

solution	R_{SOLN}(Ω)	Q_1 ($\Omega^{-1}s^n$)	n_1	R_{OSL} (kΩ)	Q_2 ($\Omega^{-1}s^n$)	n_2	R_{MSL} (kΩ)	Q_3 ($\Omega^{-1}s^n$)	n_3	R_{CT} (kΩ)
pFe = 12; $E = -30.8$ mV	neg[b]	1.9×10^{-6}	0.564	0.84	2.0×10^{-6}	0.789	15.3	2.3×10^{-5}	0.660	96.0
pFe = 10; $E = 0.8$ mV	neg	2.1×10^{-6}	0.581	0.863	1.9×10^{-6}	0.775	13.3	2.6×10^{-5}	0.591	75.9
pFe = 8; $E = 35.9$ mV	neg	2.0×10^{-6}	0.555	0.997	2.0×10^{-6}	0.757	10.5	4.0×10^{-5}	0.727	16.8
seawater $E = -159$ mV	neg	1.4×10^{-6}	0.564	1.26	4.4×10^{-6}	0.742	24.6	1.9×10^{-5}	0.574	44.2

[a] Note that $\Delta E/\Delta pFe = -17$ mV/decade, which arises as a consequence of uncertainties in citrate speciation calculations at pFe < 13, while $\Delta E/\Delta pFe \approx$ -30 mV/decade at pFe > 13, as has been reported elsewhere.[7] [b] neg, negligible.

Table 5. Boukamp Equivalent Circuit Parameters and Open Cell Potentials for a RDE Chalcogenide Fe^{III} ISE in Fe^{III}−EDTA Buffers at 3000 rpm[a]

solution	R_{SOLN} (Ω)	Q_1 ($\Omega^{-1}s^n$)	n_1	R_{OSL} (kΩ)	Q_2 ($\Omega^{-1}s^n$)	n_2	R_{MSL} (kΩ)	Q_3 ($\Omega^{-1}s^n$)	n_3	R_{CT} (kΩ)
pFe = 20; $E = -76$ mV	neg[b]	3.5×10^{-6}	0.531	1.01	2.0×10^{-6}	0.770	31.3	1.1×10^{-5}	0.568	154
pFe = 15; $E = -8.7$ mV	neg	3.2×10^{-6}	0.542	0.951	2.7×10^{-6}	0.707	22.9	1.6×10^{-5}	0.618	89.4
pFe = 10; $E = 55.1$ mV	neg	9.0×10^{-6}	0.451	0.862	1.8×10^{-6}	0.814	21.9	1.3×10^{-5}	0.528	58.0

[a] Note that $\Delta E/\Delta pFe = -13$ mV/decade, and this sub-Nernstian response has been reported elsewhere[7] for EDTA buffers at pFe < 17, while $\Delta E/\Delta pFe \approx$-30 mV/decade at pFe > 17.[7] [b] neg, negligible.

that citrate facilitates the charge-transfer process as evidenced by R_{CT} values that are much lower than those obtained in unbuffered Fe^{3+} standards (compare Table 1 with Table 4). Presumably, citrate and other complexing agents favor the kinetics of charge transfer via complexation of the products of the charge-transfer reaction, decelerating the reverse reaction of the reversible charge-transfer process, increasing the net rate. It should be noted that citrate has a moderately high affinity for Fe^{3+} (log K_{stab} = 16.96) and Fe^{2+} (log K_{stab} = 4.4).[16]

It is also significant to note that MSL impedances are quite similar in the Fe^{III}−citrate buffer compared with the results in unbuffered Fe^{3+} standards (compare Table 1 with Table 4), and the MSL impedance is relatively constant in buffers of variable pFe. This is symptomatic of a comparable ion-exchange process in citrate buffers at high pFe values, which is probably attributable to the ready exchange of Fe^{3+} from labile Fe^{III}−citrate complexes.

Table 5 presents EIS equivalent circuit parameters for a RDE Fe^{III} ISE in Fe^{III}−EDTA buffers. As expected, the charge-transfer impedance decreases at elevated levels of free Fe^{III} in the EDTA buffer. Note that the R_{MSL} value for the pFe = 10 EDTA buffer is higher than the corresponding value in citrate buffers (compare Tables 4 and 5). This indicates that EDTA impedes the ion exchange of Fe^{3+} due possibly to the formation of strong Fe^{III}− and Fe^{II}−EDTA complexes (viz., log K_{stab} = 25.0 and 14.27, respectively[16]). Notably, the charge-transfer impedance at pFe = 10 was lower in EDTA buffers, compared to citrate buffers, suggesting that the removal of reaction products from the Fe^{III} ISE surface, and its concomitant effect on the reverse reaction of the charge-transfer process, is more pronounced in the presence of EDTA.

On the other hand, seawater at pFe ≈ 19[17] yields considerably lower R_{MSL} and R_{CT} values compared to the those in the Fe^{III}−EDTA buffer at pFe = 20 (compare Tables 4 and 5). A smaller R_{MSL} value strongly suggests that the adsorption of organic ligands and Fe^{III}−organic complexes in seawater is in some way facilitating

(16) Martell, A. E.; Smith, R. *Critical Stability Constants*; Plenum Press: New York, 1977; vol. 4.

(17) Millero, F. J.; Yao, W.; Aicher, J. *Mar. Chem.* **1995**, *50*, 21−39.

Table 6. Boukamp Equivalent Circuit Parameters and Open Cell Potentials for a RDE Chalcogenide Fe^{III} ISE in Fe^{III}−Salicylate Buffers at 3000 rpm[a]

solution	R_{SOLN} (Ω)	Q_1 ($\Omega^{-1} s^n$)	n_1	R_{OSL} (kΩ)	Q_2 ($\Omega^{-1} s^n$)	n_2	R_{MSL} (kΩ)	Q_3 ($\Omega^{-1} s^n$)	n_3	R_{CT} (kΩ)
pFe = 7.2; E = −36.9 mV	neg[b]	5.0×10^{-7}	0.661	0.819	1.7×10^{-6}	0.705	16.2	1.5×10^{-5}	0.503	123
pFe = 6.2; E = −10.8 mV	200.8	1.1×10^{-8}	1.00	0.725	2.0×10^{-6}	0.706	14.7	2.3×10^{-5}	0.495	79.7
pFe = 4.7; E = 43.5 mV	neg	8.2×10^{-7}	0.626	1.08	1.7×10^{-6}	0.708	18.4	2.3×10^{-5}	0.560	51.7

[a] Note that $\Delta E/\Delta pFe = -33$ mV/decade. [b] neg, negligible.

Table 7. Boukamp Equivalent Circuit Parameters for a RDE Chalcogenide Fe^{III} ISE as a Function of pH in an Fe^{III}−EDTA Buffer at a Fixed Fe of 20, and a Rotation Speed of 3000 rpm

solution pH	R_{SOLN} (Ω)	Q_1 ($\Omega^{-1} s^n$)	n_1	R_{OSL} (kΩ)	Q_2 ($\Omega^{-1} s^n$)	n_2	R_{MSL} (kΩ)	Q_3 ($\Omega^{-1} s^n$)	n_3	R_{CT} (kΩ)
3.8	72.5	5.3×10^{-7}	0.678	0.585	9.4×10^{-7}	0.857	17.4	9.6×10^{-6}	0.570	181
4.6	95.9	2.3×10^{-7}	0.747	0.542	1.4×10^{-6}	0.803	17.1	9.5×10^{-6}	0.580	180
6.0	49.7	1.2×10^{-7}	0.770	0.379	5.8×10^{-7}	0.828	13.2	9.6×10^{-5}	0.542	169

the ion-exchange process of the Fe^{III} ISE, and the diminution in R_{CT} implies that natural organic chelating ligands in seawater are aiding in the removal of charge-transfer reaction products formed at the ISE surface, increasing the net rate of the charge-transfer reaction. Whatever the reason, the EIS results demonstrate that organic ligands exert a significant influence on the response mechanism of the Fe^{III} ISE. Most importantly, it is crucial to use a calibration ligand that mimics the effects of seawater ligands on the kinetics of the electrode reaction.

EIS spectra for a RDE Fe^{III} ISE in Fe^{III}−salicylate buffers have been fitted to the corresponding equivalent circuit elements presented in Table 6. A distinctive feature in the EIS spectra for the salicylate buffer is the lack of a trend in R_{MSL}, noting that R_{MSL} values are somewhat higher than the corresponding results in citrate buffers (compare Tables 4 and 6), suggesting that ion exchange of Fe^{3+} at the ISE surface is hindered by the presence of adsorbed salicylate and Fe^{III}−salicylate complexes. Notably, the much larger R_{CT} value for a salicylate buffer at pFe = 7.2, compared to the citrate buffer at pFe = 8, suggests that complexation of the charge-transfer reaction products by the salicylate ligand is less pronounced, favoring the reverse of the charge-transfer process, lowering the net rate.

In summary, the EIS data have shown unequivocally that buffer ligands affect the response of the Fe^{III} ISE, possibly via complexation of the products of the charge-transfer reaction. Potentiometric response studies in buffered media have shown that the variation in the standard potential ($E°$) in different ligand systems correlates with the log K_{stab} values for Fe(III) and Fe(II) complexes. More importantly, a trend was observed between EIS kinetic and potentiometric response data in the following order: EDTA > citrate > salicylate. This trend correlates strongly with the standard potentials and log K_{stab} values for Fe complexes;[16] i.e., $E°$ (EDTA) = 444 mV; $E°$ (citrate) = 228 mV; $E°$ (salicylate) = 121 mV; $\log K_{stab}(Fe^{III}-EDTA) = 25$; $\log K_{stab}(Fe^{II}-EDTA) = 14.27$; $\log K_{stab}(Fe^{III}-Hcitrate) = 16.96$; $\log K_{stab}(Fe^{II}-citrate) = 4.4$; $\log K_{stab}(Fe^{III}-salicylate) = 15.81$; $\log K_{stab}(Fe^{II}-salicylate) = 6.55$.

EIS studies on the effect of pH in buffered media were also undertaken to rule out the possibility that the Fe^{III} ISE is responding indirectly to H^+. This experiment was undertaken at a fixed pFe of 20 that was achieved through alteration of the Fe^{3+}-to-EDTA ratio along with the pH.

EIS equivalent circuit parameters for a RDE Fe^{III} ISE in saline EDTA buffers at a constant pFe of 20 and variable pH are presented in Table 7. The similarity in R_{MSL} and R_{CT} values clearly shows that the kinetics of ion-exchange and charge-transfer processes are independent of pH. Furthermore, the potentiometric response was also independent of pH. These results demonstrate unequivocally that a variation in pH in metal buffers alters the concentration of Fe^{3+} that the electrode senses, not pH. The slight variation in EIS Nyquist plots is equivalent to a difference in R_{CT} of approximately 5−10%, which is commensurate with the repeatability of the EIS technique, while the more significant variations of about 10−20% in R_{OSL} and R_{MSL} are due to inaccuracies in the Boukamp equivalent circuit fitting procedure when small high-frequency impedances (e.g., R_{OSL} and R_{MSL}) are deconvoluted from much larger low-frequency impedances (viz., R_{CT}).

It is important to note that Q values for the OSL and CT elements varied more significantly as a function of pH at constant pFe, as compared to all other Fe buffer data that originate from variations in pFe by altering the pH (compare Table 7 with Tables 4−6). This may be due to blocking of the interface by an iron oxide and/or iron hydroxide film at elevated pH, which has an impact on the CPE values for the OSL and CT elements, and/or it is attributable to imperfections in the surface states of the chalcogenide glass, which is the ultimate cause of CPEs, and these effects may be variable from experiment to experiment whereby the ISE is repolished on each occasion. On a related point, it is expected theoretically that these Q values will be independent of $[Fe^{3+}]$, but the EIS data (see Tables 4−6) reveal that there are slight variations in Q as the concentration of Fe^{3+} is altered in unbuffered and buffered media. Considering that pFe in buffered media is varied by altering the solution pH, it is conceivable that a blocked interface by iron oxide and/or iron hydroxide may also be responsible for this behavior, albeit that there is some uncertainty about the variation in Q being attributed to surface imperfections arising from repolishing of electrodes.

Table 8. Boukamp Equivalent Circuit Parameters for a RDE Chalcogenide Fe^{III} ISE as a Function of Voltage Amplitude in 10^{-2} M $FeCl_3$ at a Rotation Speed of 1,000 rpm

voltage amplitude (mV)	R_{SOLN} (Ω)	Q_1 (Ω^{-1} s^n)	n_1	R_{OSL} (kΩ)	Q_2 (Ω^{-1} s^n)	n_2	R_{MSL} (kΩ)	Q_3 (Ω^{-1} s^n)	n_3	R_{CT} (MΩ)
±5	neg[a]	7.2×10^{-10}	1.00	0.862	3.2×10^{-7}	0.954	141	1.1×10^{-6}	0.498	2.91
±10	neg	4.1×10^{-10}	1.00	1.12	3.2×10^{-7}	0.952	137	1.1×10^{-6}	0.482	3.09

[a] neg, negligible.

The EIS impedance data have been validated in unbuffered and buffered media using Kramers−Kronig transformations. This approach to EIS data analysis demonstrates whether the EIS data satisfy the linear systems theory (i.e., conditions of causality, linearity, and stability are fulfilled). Figure 4 presents Kramers−Kronig transformations for the Fe^{III} ISE in pFe = 10 citrate buffer: (a) transform of real to imaginary impedances; (b) transform of imaginary to real impedances. The very good agreement between actual log(Z') and log(Z'') and corresponding values estimated using Kramers−Kronig transformations demonstrates that the Kramers−Kronig relations hold, and the impedance data are free from artifacts and/or errors. It is worth noting that the small deviations at the extremities in frequency response are probably due to data errors arising from stray capacitances and electrode instability at high and low frequencies, respectively.

Macdonald's[14] seminal EIS textbook indicates that the linear systems theory should hold for ac voltage amplitudes of ±25 mV. We therefore studied the EIS response of the Fe^{III} ISE as a function of ac voltage amplitude (see Table 8 for equivalent circuit fits). Although the Kramers−Kronig transformations validated the EIS data at an ac voltage amplitude of ±10 mV, the deviations in some circuit parameters of ±5−15% for voltage amplitudes of ±5 and ±10 mV demonstrate that the reproducibility of the EIS method is degraded by instability in the Fe^{III} ISE, as evidenced by a drift of 1−10 mV over the duration of EIS measurements. On this point, we and Koenig and Grabner[5] have noted that a polished Fe^{III} ISE ages significantly in aqueous media, and this alters the EIS response of the system. Consequently, it was deemed necessary to equilibrate the Fe^{III} ISE for 2 days in the electrolyte in order to stabilize the system, yielding the reproducible EIS spectra at variable voltage amplitudes.

XPS Studies. Mechanistic aspects of the Fe^{III} ISE have been investigated by carrying out XPS analyses of membranes exposed to various saline solutions. Importantly, the XPS study was undertaken to identify the OSL and MSL surface films that have been detected in the aforementioned EIS study of the Fe^{III} ISE.

Figure 5a presents the Fe(2p) XPS spectrum for a polished chalcogenide membrane after argon ion etching for 200 s, noting that the polished sample's spectrum (not shown) failed to detect any Fe in the surface layers of the membrane. Respectively, the binding energies of the detected Fe($2p_{3/2}$) and Fe($2p_{1/2}$) spin−orbit split components at 707 and 721 eV are consistent with Fe in FeSe or metallic Fe.[18] The broad and unresolved nature of the peaks made it difficult to discriminate between different Fe species on the surface, and the use of argon ion etching probably complicated matters further by inducing ion beam artifacts. In any event, the fact that the surface layers of the polished membrane are depleted with respect to Fe strongly suggests that a MSL exists on the surface of the ISE, and in fact, Koenig's and Grabner's[5] XPS depth profile demonstrated that the thickness of the MSL is ∼8 nm.

Table 9. XPS Binding Energies (eV) of Different Core Levels for Fe^{III} ISE Membranes Exposed to Various Saline Solutions

level	etched[a]	Fe^{III}−EDTA[b]	seawater[c]
Fe($2p_{3/2}$)	707.0	nd[d]	nd
Fe($2p_{1/2}$)	721.0	nd	nd
Ge($2p_{3/2}$)	1218.5	1218.9; 1220.1	1218.7; 1220.1
Sb($3d_{5/2}$)	529.1	529.4; 530.9	528.8; 530.9
Sb($3d_{3/2}$)	538.4	538.7; 540.1	538.1; 539.7
Se($3d_{5/2}$)	53.9	53.9	53.6; 55.4
Se($3d_{3/2}$)	54.8	54.8	54.3
C(1s)	284.4	284.7	284.4

[a] Polished and argon ion etched for 200 s. [b] Exposed to saline Fe^{III}−EDTA buffer at pFe = 20 for 3 days. [c] Exposed to seawater for 3 days. [d] nd, not detected..

Significantly, Fe was not detected on the surface of a polished membrane that had been exposed to a saline Fe^{III}−EDTA solution for 3 days (see Figure 5b and Table 9). It is also important to note that the C(1s) peaks (see Table 9) that are associated with carboxylate and amine groups in EDTA were not detected in the C(1s) XPS spectrum of this sample; however, the peak at ∼284.7 eV is attributable to adventitious hydrocarbons. Likewise, the membrane exposed to seawater for 3 days failed to detect any Fe or adsorbed carboxylate species that are assignable to humates/fulvates at the membrane surface. These results demonstrate that the surface layers of the chalcogenide glass membrane are depleted with respect to Fe, noting that physisorbed ligands, if present, are desorbed during rinsing with water. The presence of an Fe-deficient MSL is internally consistent with the EIS data, which revealed a high impedance film (i.e., R_{MSL}), noting that Koenig and Grabner[5] have shown that the bulk impedances of iron chalcogenide glass membranes increase at lower levels of iron. Notably, the XPS results show that the MSL is formed during polishing and rinsing with water, and this film is probably responsible for the selective ion exchange of Fe^{3+} at the electrolyte/electrode interface.

The XPS spectrum of the Ge($2p_{3/2}$) level for a polished and argon ion-etched membrane revealed a single peak at 1218.5 eV, which is at a higher binding energy than elemental Ge (viz., 1217 eV).[18] These XPS data demonstrate that Ge in the membrane is present as either GeSe or $GeSe_2$.[18] The Ge($2p_{3/2}$) spectrum for a polished membrane after exposure to saline Fe^{III}−EDTA at pFe

(18) *Handbook of X-ray Photoelectron Spectroscopy*; Moulder, J. F., Stickle, W. F., Sobol, P. E., Bombden, K. D., Eds.; Perkin-Elmer: Eden Prairie, MN, 1992.

20 for 3 days (see Table 9) also revealed the presence of germanium oxide (probably GeO_2) as indicated by a broad high binding energy shoulder at 1220.1 eV.[18] Similarly, the membrane exposed to seawater for 3 days also showed the presence of a high binding energy shoulder that is attributable to GeO_2 (see Table 9).

These results demonstrate that oxidation of the membrane is a contributing factor in the formation of the OSL and MSL. The formation of germanium oxide on the surface of the membrane is consistent with the presence of a solid-state material that may provide a pathway for ionic conduction, i.e., the formation of a crystalline solid with metal defect vacancies that may allow the transportation of Fe^{III} ions. It has been suggested that oxidation of the chalcogenide glass is kinetically hindered due to the amorphous structure of the membrane,[5] but the present XPS data show that the formation of a ionic solid (i.e., GeO_2) is expected to allow some Fe^{3+} ionic conductivity in this overlayer of ionic material. This hypothesis is supported by the EIS data that showed a decrease in R_{OSL} and R_{MSL} at elevated levels of Fe^{3+}, which is internally consistent with Fe^{3+} undergoing ion exchange on and within the electrolyte/membrane interface.

Respectively, the $Sb(3d_{5/2})$ and $Sb(3d_{3/2})$ spin−orbit split components for a polished and argon ion-etched Fe^{III} ISE membrane at 529.1 and 538.4 eV are probably attributable to an antimony selenide species.[18] By contrast, exposure of a membrane to saline Fe^{III}−EDTA solution for 3 days (see Table 9) revealed broad high binding energy shoulders on the Sb (3d) peaks at 530.9 and 540 eV, signifying the presence of Sb_2O_3 and/or Sb_2O_5.[18] Note, the Sb(3d) spectrum for the seawater-treated membrane (see Table 9) was identical to that for a membrane exposed to saline Fe^{III}−EDTA buffer [viz., high binding energy Sb_2O_3 and/or Sb_2O_5 shoulders were evident on the antimony selenide Sb(3d) peaks]. Significantly, antimony has undergone a surface oxidation reaction similar to germanium. Presumably, the formation of crystalline antimony oxide enables the ionic conduction of Fe^{3+}, allowing Fe^{3+} to undergo ion exchange in the OSL and MSL.

The binding energies of Se(3d) levels for the chalcogenide glass membrane are also presented in Table 9. The Se(3d) XPS spectrum for a polished and argon ion-etched surface revealed $Se(3d_{5/2})$ and $Se(3d_{3/2})$ spin−orbit split components at 53.9 and 54.8, respectively. The positions of these peaks are indicative of Se in a selenide (e.g., GeSe, $GeSe_2$, FeSe, etc).[18] No significant changes were evident in the Se(3d) spectra after treatment in a saline Fe^{III}−EDTA buffer. By contrast, exposure to seawater for 3 days demonstrated a dramatic increase in the selenide peak intensity along with a distinct shoulder at high binding energy (55.4 eV) that corresponds to elemental Se.[18] This observation may be consistent with EIS data that revealed unusually low MSL and charge-transfer impedances in seawater, indicating that seawater constituents may have oxidized some of the selenide to selenium, increasing the rate of charge transfer.

In summary, the XPS results demonstrate that surface oxidation of antimony and germanium facilitate the combined ion-exchange and charge-transfer processes that govern the Fe^{3+} response of the Fe^{III} ISE. Importantly, XPS has demonstrated that an Fe-deficient MSL can be formed either during polishing of the ISE or on exposure to saline solution, and an OSL of oxides of germanium and antimony forms on the surface of the chalcogenide glass. It may be possible that some of the redox-active constituents of seawater are oxidizing some of the membrane selenide sites to selenium, contributing to a serious interference in seawater.

Response Mechanism of the Fe^{III} ISE. It can be shown that a melding of the charge-transfer mechanism proposed by Koenig and Grabner[5] along with a conventional Fe^{3+} ion-exchange mechanism is internally consistent with the potentiometric response data of the Fe^{III} ISE. Moreover, the XPS evidence strongly supports the EIS assignment of OSL and MSL impedances, and trends in EIS kinetic data for charge transfer in unbuffered and buffered media (i.e., R_{CT} decreases or rate of charge transfer increases at elevated $[Fe^{3+}]$) are self-consistent with Koenig and Grabner's[5] charge-transfer component of the Fe^{III} ISE response mechanism.

Figure 6 summarizes the response mechanism of the chalcogenide glass membrane. When the membrane is in contact with a solution containing Fe^{3+}, an exchange of Fe^{3+} ions occurs between the electrolyte, OSL, and MSL along with semi-infinite linear diffusion of Fe^{3+} through the OSL (as supported by $n \approx 0.5$ for the CPE of the OSL), resulting in the introduction of holes (i.e., h^+) that migrate to the bulk of the chalcogenide glass. The h^+'s are inserted into the Fermi level whereby electrons from the reference electrode fill these holes (Koenig and Grabner[5]). This mechanism is indeed consistent with the EIS results that demonstrated a diminution in R_{OSL}, R_{MSL}, and R_{CT} at elevated Fe^{3+} levels. This mechanism implies that oxidation of the membrane produces OSL and MSL films that provide vacancies for Fe^{3+} migration in and out of the OSL, with XPS revealing that treated membrane surfaces comprise some oxides of germanium and antimony that presumably promote the ion exchange and conduction of Fe^{3+}. In addition, EIS data demonstrate that ion exchange of Fe^{2+} is less favorable and is probably attributable to Fe^{2+} not satisfying the size/charge requirements of the oxidized surface.

Further credence to the EIS/XPS model for the Fe^{III} ISE response mechanism is the proceeding mathematical formulation of a Nernst equation that correctly predicts the observed potentiometric response behavior of the Fe^{III} ISE.

The following electrochemical and ion-exchange reactions depict the processes occurring at the MSL of the Fe^{III} ISE, viz.

$$\text{ion exchange:} \qquad Fe^{3+}(aq) \rightarrow Fe^{3+}(MSL) \qquad (1)$$

and

$$\text{charge transfer:} \qquad Fe^{3+}(MSL) + e^- \rightarrow Fe^{2+}(MSL) \qquad (2)$$

The Nernst equation for ion exchange (i.e., reaction 1) is given by

$$E_{ionic} = E^{o}_{ionic} + \frac{2.303RT}{3F} \log(aFe^{3+}_{MSL}) \qquad (3)$$

Expansion of eq 3 yields

$$E_{\text{ionic}} = E^{\text{o}}_{\text{ionic}} + \frac{2.303RT}{3F}\log\{\gamma(\text{Fe}^{3+})\} + \frac{2.303RT}{3F}\log([\text{Fe}^{3+}]_{\text{MSL}}) \quad (4)$$

where the first two terms of eq 4 contribute to the apparent standard electrode potential for ion exchange, noting that $[\text{Fe}^{3+}]_{\text{MSL}}$ can be derived using the equilibrium constant for ion exchange and may be substituted into eq 4, viz:

$$K = \frac{[\text{Fe}^{3+}]_{\text{MSL}}}{[\text{Fe}^{3+}]} \quad (5)$$

and

$$[\text{Fe}^{3+}]_{\text{MSL}} = K[\text{Fe}^{3+}] \quad (6)$$

leading to eq 7 at constant ionic strength:

$$E_{\text{ionic}} = E^{\text{o}}_1 + \frac{2.303RT}{3F}\log\{[\text{Fe}^{3+}]\} \quad (7)$$

where

$$E^{\text{o}}_1 = E^{\text{o}}_{\text{ionic}} + \frac{2.303RT}{3F}\log\{\gamma(\text{Fe}^{3+})\} + \frac{2.303RT}{3F}\log(K)$$

On the other hand, the Nernst equation for charge transfer (i.e., reaction 2) is

$$E_{\text{electronic}} = E^{\text{o}}_{\text{electronic}} - \frac{2.303RT}{F}\log\left\{\frac{\text{aFe}^{2+}_{\text{MSL}}}{\text{aFe}^{3+}_{\text{MSL}}}\right\} \quad (8)$$

Expansion and inclusion of activity coefficients along with collection of constants in eq 8 yields eq 9:

$$E_{\text{electronic}} = E^{\text{o}}_{\text{electronic}} - \frac{2.303RT}{F}\log\{\gamma(\text{Fe}^{2+})\} + \frac{2.303RT}{F}\log\{\gamma(\text{Fe}^{3+})\} - \frac{2.303RT}{F}\log([\text{Fe}^{2+}]_{\text{MSL}}) + \frac{2.303RT}{F}\log([\text{Fe}^{3+}]_{\text{MSL}}) \quad (9)$$

Noting that the first four terms of eq 9 make up the apparent standard electrode potential for electron transfer (i.e., E^{o}_2). The Nernst equation now becomes

$$E_{\text{electronic}} = E^{\text{o}}_2 + \frac{2.303RT}{F}\log([\text{Fe}^{3+}]_{\text{MSL}}) \quad (10)$$

Substitution of eq 6 into eq 10 yields

$$E_{\text{electronic}} = E^{\text{o}}_3 + \frac{2.303RT}{F}\log([\text{Fe}^{3+}]) \quad (11)$$

where

$$E^{\text{o}}_3 = E^{\text{o}}_2 + \frac{2.303RT}{F}\log(K)$$

The steady-state potentials of the ionic and electronic processes are in equilibrium at a combined potential E_+, which is evaluated by summing the electrochemical potentials (i.e., μ), viz:

$$\mu_{\text{combined}} = \mu_{\text{electronic}} + \mu_{\text{ionic}} = (-z_{\text{electronic}}FE_+) + (-z_{\text{ionic}}FE_+) \quad (12)$$

Using eq 12 in conjunction with eqs 7 and 11 leads to

$$E_+ + 3E_+ = E_{\text{electronic}} + 3E_{\text{ionic}} = E^{\text{o}}_3 + 3E^{\text{o}}_1 + \frac{2.303 \times 2RT}{F}\log([\text{Fe}^{3+}]) \quad (13)$$

Rearrangement of eq 13 yields the Nernst equation, which describes the combined potential, viz:

$$E_+ = \frac{(E^{\text{o}}_3 + 3E^{\text{o}}_1)}{4} + \frac{2.303RT}{2F}\log([\text{Fe}^{3+}]) = E^{\text{o}}_+ + \frac{2.303RT}{2F}\log\{[\text{Fe}^{3+}]\} \quad (14)$$

It can be seen that eq 14 predicts a Nernstian slope of 29.6 mV/decade change in $[\text{Fe}^{3+}]$, which closely matches the experimentally determined slope of 27−34 mV/decade. This mechanism also implies that the potential is independent of $[\text{Fe}^{2+}]$ as the level of divalent ion in the electrode's diffusion layer is dictated by the solubility of the membrane phase comprising mostly Fe^{2+}, and this only affects the E^{o} of the electrode (see eq 9). In fact, the EIS data have shown that, although the charge-transfer and ion-exchange processes are facilitated at elevated levels of $[\text{Fe}^{2+}]$, the effect with Fe^{2+} is less pronounced than that observed with Fe^{3+}.

CONCLUSIONS

The results of this study demonstrate unambiguously that the response mechanism of the Fe^{III} ISE is based on a combination of ion exchange and charge transfer at the electrolyte/electrode interface. A significant outcome of the theory on electrode response is the suggestion that a reliable ISE analysis of seawater may be possible if the Fe^{III} calibration buffer comprises a ligand of comparable Fe^{II} and Fe^{III} complexing capacities of natural organic ligands in seawater (i.e., humic and fulvic acids). Although there is little knowledge on the Fe^{II} complexing capacity of seawater ligands, it may be possible to use a matrix modifier in seawater and calibration buffers that selectively complexes the

Fe^{II} in the electrode's diffusion layer, yielding identical electrode standard potentials in both media.

ACKNOWLEDGMENT

The authors are indebted to Professor J. Ross Macdonald of the Department of Physics and Astronomy at the University of North Carolina, who kindly performed Kramers−Kronig transformations on some of our EIS data. We also thank Dr. Denis Mackey of the CSIRO Division of Marine Research for useful discussion on the response of the Fe^{III} ISE in seawater along with the donation of some seawater samples, and Dr. Alberto Zirino of SPAWAR Systems Center San Diego for providing valuable feedback on the proposed mechanism. The financial support of the Australian Research Council (ARC) is gratefully acknowledged.

Received for review June 9, 1999. Accepted October 27, 1999.

AC990603X